Carbon 139, 872-879 (2018)

Synergism of nitrogen and reduced graphene in the electrocatalytic behaviour of resorcinol - formaldehyde based carbon aerogels

Balázs Nagy[1], István Bakos[2], Imre Bertóti[2], Andrea Domán[1], Alfréd Menyhárd[1], Miklós Mohai[2], Krisztina László[1]

[1]Department of Physical Chemistry and Materials Science, Budapest University of Technology and Economics, H-1521 Budapest, PO Box 91, Hungary

[2]Institute of Materials and Environmental Chemistry, Research Centre for Natural Sciences, Hungarian Academy of Sciences, H-1519 Budapest, PO Box 286, Hungary

Abstract

Graphene oxide (GO) containing resorcinol – formaldehyde and resorcinol – formaldehyde – melamine polymer aerogels were converted to carbon aerogels in order to study the cooperative effect of the reduced GO and nitrogen functionalities on the electrochemical behavior of carbon aerogels. The morphology of the carbon gel was characterized by scanning and transmission electron microscopy, and low temperature nitrogen adsorption/desorption. X-ray photoelectron spectroscopy was used to study their surface chemistry. The thermal behavior was investigated by thermogravimetric analysis. The electrochemical performance was tested with cyclic- and linear sweep voltammetry (CV and LSV, respectively). The final N content was ca 1 atomic%. The nitrogen atoms are in a C=N-C type chemical environment or replace a carbon atom in the graphene-like layer. Either N or the reduced GO enhance the activity in oxygen reduction reaction. When both are present in the matrix the dominant reduction pathway changes from the slow $2e^-$ to the more efficient $4e^-$ route. It is also probable that the *in-situ* formed H_2O_2 improves the wettability of the basically hydrophobic carbon surface and increases the electrochemically active surface.

Keywords: carbon aerogel, doping, graphene oxide, oxygen reduction reaction

[1] Corresponding author. Department of Physical Chemistry and Materials Science, Budapest University of Technology and Economics, H-1521, Budapest, Hungary. E-mail address: klaszlo@mail.bme.hu (K. László).

1. Introduction

In response to the harmful effects of conventional energy sources and the depletion of non-renewable energy sources there is an increasing demand to develop alternative environmentally friendly energy sources [1]. Fuel cells seem promising alternatives. These devices can convert chemical energy efficiently into electrical energy via the chemical reaction of fuel (e.g. hydrogen, methanol) with oxygen or other oxidants [2]. The H_2/O_2 fuel cell is the type that is currently most intensively studied [3]. In general, a fuel cell consists of two electrodes in contact with a conductive electrolyte layer. Fuel is fed continuously to the anode side, while the oxidant is fed to the cathode. In the case of proton exchange fuel cells (PEMFCs) [4] and microbial fuel cells (MFCs) [5], Pt-based materials are the most active catalysts as cathodes in the oxygen reduction reaction (ORR). Their outstanding catalytic activity in the ORR is attributed to the fast, 4-electron pathway. A further advantage is their lack of formation of any corrosive H_2O_2 intermediate [6].

Possible cathode reactions:

I. 4-electron pathway: $O_2 + 4H^+ + 4e^- \rightarrow 2H_2O$

II. 2-electron pathway: $O_2 + 2H^+ + 2e^- \rightarrow 2H_2O_2$

$H_2O_2 + 2H^+ + 2e^- \rightarrow 2H_2O$

The cathode reactions are too slow without Pt catalysis, but the expense of the required Pt loading is an obstacle to commercializing these fuel cells. To avoid this difficulty, an intense research effort is directed into replacing the Pt-based catalysts of the cathode by more economical, durable materials of sufficient activity [7–10].

In this work we focus on the potential of nitrogen and graphene inclusion. Low-cost, environmentally friendly nitrogen doped carbon-based systems with excellent electro-catalytic activity are promising alternatives for this purpose [11]. It has been shown that nitrogen atoms incorporated into carbon materials significantly increase the catalytic activity of high surface area carbon materials [12,13]. The C-N structure also has an important role in the ORR activity [14–18].

Nitrogen can be incorporated into the carbon structure in various chemical forms, mainly as graphitic, pyrrolic, pyridinic or oxidized pyridinic species [19–21]. Graphitic nitrogens replace carbon atoms in the lattice. Being bonded to three carbon atoms they increase the number of electrons in the delocalised π electron system. Pyrrolic and pyridinic nitrogen atoms are situated at the edges and at defects of the carbon structure, each N atom being bonded to two carbon atoms in 5 and 6-membered rings, respectively. The role of nitrogen atoms with different

bonding states in the ORR activity is not clear, but most often the enhanced activity is attributed to the graphitic and/or pyridinic nitrogen atoms [4,14,21].

There are numerous ways of obtaining N-containing carbons. They can be produced from nitrogen-rich natural (chitosan, glucosamine, chitin) [22,23], or synthetic (polyurethane, polyamide, polyacrylonitrile (PAN)) [24–27], polymers. It is also possible to incorporate N atoms into the structure via the chemical post-treatment of the carbon materials, e.g., by applying N containing gases (NH_3, $(CN)_2$) during carbonization [28] or impregnation with urea or melamine [29,30] followed by thermal treatment. Other methods, for example NH_3 or low pressure N_2 plasma treatment [31,32] are also employed.

For more than two decades sol-gel techniques have been applied to prepare polymer aerogels with tailored structure, which are excellent precursors for porous carbons [33], so-called carbon aerogels. Resorcinol (R) and formaldehyde (F) have been the most widely used monomers, but nitrogen containing monomers such as melamine (M) [21,34,35], urea [36], L-lysine [37], 3-aminophenol [38], 3-hydroxi pyridine [34], 3-hydroxianiline [34], etc. can also be used to obtain nitrogen containing carbon materials.

High electrical conductivity of the fuel cell catalyst is important to minimize ohmic losses associated with the electron transfer [39], i.e., the improved electrical conductivity of the carbon support is beneficial. Incorporating graphene particles into the carbon aerogel matrix may effectively increase the electrical conductivity [40–42]. The introduced graphene enhances further electrochemical properties of such carbons, as the capacity [40,41,43–45] or the activity in ORR [46].

In our previous work on the electrocatalytic properties of resorcinol-melamine-formaldehyde (RMF) polymer based carbon aerogels [21] it was reported that the nitrogen content from melamine improved the electrochemical features of the aerogel. Based on the above cited references, further enhancement is feasible by incorporating graphene derivatives into the RMF matrix prior to the carbonization. The aim of the present work is to examine the cooperative effect of graphene and nitrogen doping on the electrochemical behavior of carbon aerogels. For this purpose, graphene oxide containing resorcinol – formaldehyde (RF) and RMF polymer gels were synthesized and converted to carbon aerogels. The morphology of the carbon gel was characterized by scanning and transmission electron microscopy (SEM, TEM), and low temperature nitrogen adsorption/desorption. X-ray photoelectron spectroscopy (XPS) was used to study their surface chemistry and thermogravimetry (TGA) was employed to determine the thermal behavior. The electrochemical performance was tested with cyclic- and linear sweep voltammetry (CV and LSV, respectively).

2. Experimetal

2.1. Materials

A ca. 1 wt% aqueous suspension of graphene oxide (GO) was prepared from natural graphite (Graphite Tyn) by the improved Hummers' method [47].

RF hydrogels were prepared by the aqueous polycondensation reaction of resorcinol (R) and formaldehyde (F) by the method of Lin and Ritter [48]. Briefly, R (Merck), F (37% in water, Merck) and the catalyst sodium carbonate (99%, Merck) were dissolved in distilled water with molar ratios R/F = 0.5 and R/Na_2CO_3 = 50. The overall concentration was 5 wt%. The initial pH of the solution was adjusted to pH 6.0 with dilute HNO_3 (Merck). The RF sol was kept at 85 °C for 1 week to complete the gelation. After solvent exchange, the hydrogels were dried with supercritical CO_2. RF carbon aerogels were obtained from the polymer aerogels by carbonization in dry N_2 atmosphere at 900 °C. A detailed description of the synthesis is given elsewhere [49]. The GO containing gel was prepared by replacing the distilled water by a dilute GO suspension. RMF gels were obtained in a similar way but melamine (M, Merck) was also included in the precursor solution. R, M and the catalyst were dissolved in distilled water at 70 °C, than F was added to the solution. The molar ratios were M/R = 0.2, R/Na_2CO_3 = 50, F = (2R + 3M). The initial pH was measured, but not adjusted. Further steps of the synthesis are the same as in case of RF. Detailed conditions are given in our previous work [21]. The composition of the precursor solutions and the nomenclature of the carbon aerogels are listed in Table 1.

Table 1. Composition of precursor solutions and the polymer to carbon yield

Polymer sample	R/W mg/ml	R/Na_2CO_3 molar ratio	M/R molar ratio	GO/R mass ratio	Initial pH	Expected yield* (%)
RF	33.31	50	0	-	6.0	47.5
RFG	33.31	50	0	0.1	6.0	45.8
RMF	33.31	50	0.2	-	6.8	42.1
RMFG	33.31	50	0.2	0.1	6.2	46.1

* of polymer to carbon conversion, from thermal analysis

The GO was characterized in monolithic form, prepared by unidirectional freeze drying [50]. Reduced graphene oxide (RGO) was obtained by thermal reduction of the monoliths (900 °C, Ar atmosphere, yield: ca 35 %), which resulted in a drop of the oxygen content from 34.5 to 16.9 at%.

2.2. Methods

Thermogravimetric analysis (TGA) was performed on a Perkin Elmer STA-6000 apparatus. The samples were placed in alumina crucibles and heated from room temperature to 900 °C at a heating rate of 10 °C /min under a flow of nitrogen (20 mL/min) as purge gas. The texture of the samples was characterized by scanning and transmission electron microscopy (SEM and TEM, respectively) (Hitachi SU8030 and JEM2100). Nitrogen adsorption/desorption isotherms were measured at -196 °C with a Nova2000e (Quantachrome) computer controlled apparatus. Transformation of the primary adsorption data and pore size analysis were performed with the QuantachromeASi Qwin software (version 3.0). The apparent surface area S_{BET} was calculated using the Brunauer–Emmett–Teller (BET) model. The total pore volume ($V_{0.95}$) was derived from the amount of nitrogen adsorbed at relative pressure 0.95, assuming that the pores are then filled with liquid adsorbate. The micropore volume (W_0) was derived from the Dubinin–Radushkevich (DR) plot. The pore size distribution (PSD) was calculated using quenched solid density functional theory (QSDFT) assuming slit shaped pores. Water vapour adsorption isotherms were measured on a volumetric Hydrosorb apparatus (Quantachrome) at 20 °C. The contact angles were measured with water on a Drop Shape Analysis System (DSA30, KRÜSS GmbH) using the sessile drop method and the drop-build-up technique.

The chemical composition of the surfaces was analysed by X-ray photoelectron spectroscopy using a Kratos XSAM 800 spectrometer operating in fixed analyzer transmission mode, using Mg $K\alpha_{1,2}$ (1253.6 eV) excitation. A Gaussian-Lorenzian peak shape (70/30 ratio) was used for peak decomposition [32]

Glassy Carbon (GC) Rotating Disc Electrode (RDE) and Rotating Ring-Disc Electrode (RRDE) (GC disc and Pt ring) were used for the electrochemical measurements. The working electrodes were prepared by dispersing 2 mg of powdered carbon samples in 2 mL mixture of 1.6 mL of MilliQ water, 0.4 mL isopropyl alcohol and 8 μL 5% Nafion® solution. The suspension was sonicated for 30 min. From this suspension a drop was pipetted on to the dry mirror-polished GC and dried at room temperature. In all cases 50 $\mu g/cm^2$ loading was used. Measurements were made in 0.5 M H_2SO_4 electrolyte with a three-electrode system employing a hydrogen electrode and Pt wire as reference and counter electrodes respectively. All potentials are given in RHE scale.

3. Results and discussion

3.1. Characterisation of the samples

TGA was used to study the thermal conversion of the polymer samples and GO (see Fig S1 in the Supplementary material). Both RF (Fig. S1a) and RMF (Fig. S1b) have a multistep

decomposition, in which two main steps are revealed on the differential thermogravimetric (DTG) curves around 350 and 550 °C respectively. The ratio of the mass losses corresponding to the two steps, however, is considerably different in the case of the two polymers. The second, at 550 °C (usually related to the decomposition of C-O bonds), is the dominant step in the case of the RF sample, but the intensity of this step is, in contrast, much smaller in the case of the RMF sample. Here the thermal degradation of the N-containing groups overlaps with that of the C-H bonds [51].The added GO has practically no influence on the TG signal of either the RF or the RMF polymers. The characteristic sharp peak of GO related to CO_2 release around 200 °C is missing from the corresponding DTG curves [52]. Nevertheless, this CO_2 may act as an internal activating agent during the pyrolysis of the polymers.

The SEM and TEM micrographs (Fig 1.) show the typical loosely interconnected structure and complex porosity of the carbon aerogels. The graphene-like sheets are well dispersed and clearly identifiable in the carbon aerogel matrix, as also reported in Refs 53,54. The graphene layers are completely covered by the aerogel beads, which suggests good compatibility between the nanoparticle and the hydrogel being formed during the sol-gel process.

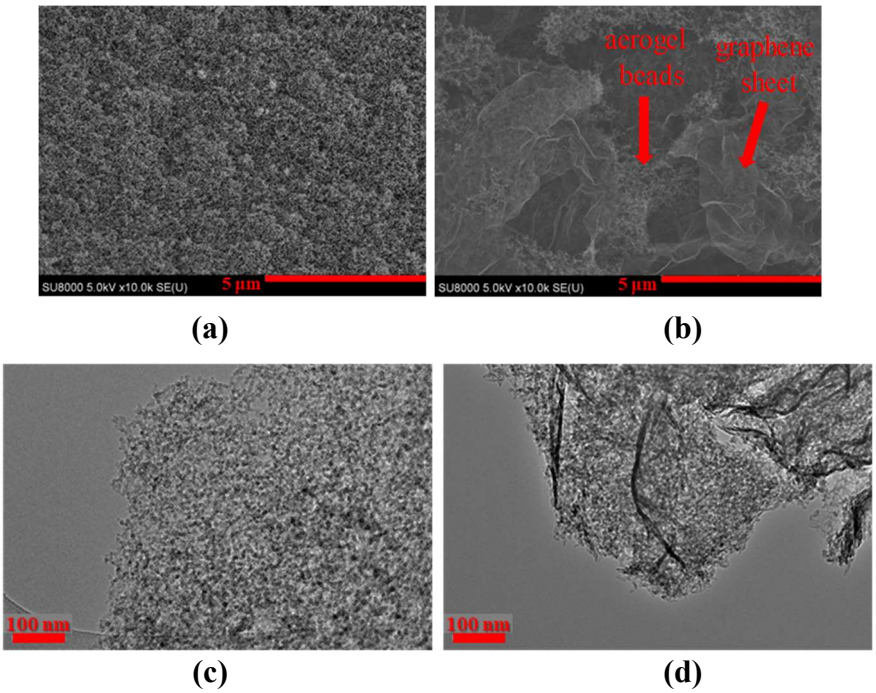

Fig.1. SEM (a,b) and TEM (c,d) images of RFC (a,c) and RFGC (c,d) samples

The Type IV low temperature nitrogen adsorption isotherms of the polymer aerogels reveal a network of micro-, meso- and macropores (Fig. 2a) [55]. The adsorption isotherm of the freeze dried GO monolith is of type II, commonly attributed to nonporous or macroporous adsorbents [55]. This means that there are hardly any measureable pores between the GO layers.

The significant change of its isotherm indicates that during the heat treatment, besides the possible CO_2 release, further exfoliation may occur [52].

As expected, the shape of the carbon aerogel isotherms (Fig 2b) is conserved [49], but the enhancement in the initial sections as well as in the apparent surface area implies development of further micropores (Table 2). The added GO has a stronger influence on the RMF based carbon, without any significant influence on the pore structure in the micro- and mesoporous regions (Fig 2c.). According to the PSD curves the typical pore sizes are similar in all the carbon aerogels.

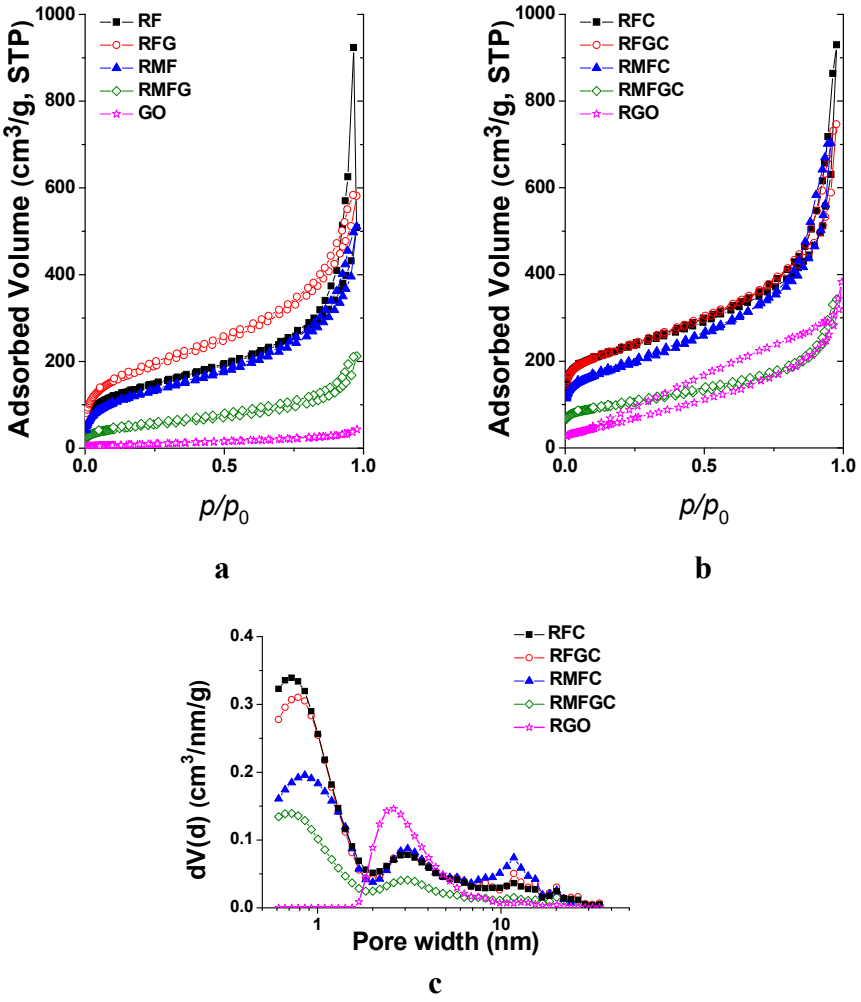

Fig. 2. Low temperature (-196 °C) nitrogen adsorption/desorption isotherms of the non-carbonized (a) and carbonized (b) samples and the pore size distributions of the latter (c) calculated by QSDFT, slit/cylinder geometry

Table 2. Data deduced from low temperature nitrogen adsorption measurements

Samples		S_{BET}[a]	$V_{0.95}$[b]	W_{0DR}[c]
		m^2/g	cm^3/g	cm^3/g
Precursors	GO	36	0.06	0.01
	RF	503	0.67	0.18
	RFG	637	0.79	0.22
	RMF	444	0.61	0.15
	RMFG	185	0.26	0.07
Carbons	RGO	230	0.40	0.06
	RFC	823	0.98	0.33
	RFGC	812	0.91	0.33
	RMFC	645	0.87	0.28
	RMFGC	358	0.44	0.14

[a]Surface area from BET model; [b] pore volume at $p/p_0 = 0.95$; [c] micropore volume from DR model

The surface composition of the carbon samples was determined by XPS (Table 3.). Although both composite samples have slightly higher oxygen content than the GO free samples, the difference is not significant, implying that the GO is reduced during the heat treatment. The N-content introduced via the melamine addition was ca. 1 atomic% after the carbonization. Only two nitrogen species N1 and N2 were found in RMFC and RMFGC samples at 398.3 and 400.9 eV, respectively. The N1 peak component can be identified as C=N-C type chemical environment, where the sp^2 nitrogen is bonded to two sp^2 type carbons, as in pyridine [32]. The N2 type at 400.9 eV is attributed to N substituting carbon in a graphite-like environment. This suggests that only the polyaromatic ring of the melamine survives the heat treatment, and the $–NH_2$ functional groups vanish. The N2 form is dominant in both nitrogen containing samples. Although there is no agreement in the literature about which particular form of nitrogen is active in ORR, both N1 and N2 were found to be advantageous [16].

Table 3. Surface composition of the carbon samples from XPS analysis (atomic%)

Carbon sample	O	C	N1	N2
RFC	1.7	98.3	-	-
RFGC	2.2	97.8	-	-
RMFC	1.5	97.5	0.3	0.7
RMFGC	1.6	97.8	0.2	0.5
RGO	16.9	83.1	-	-

The electrical conductivity (DC) was measured to estimate the overall effect of the nitrogen and GO incorporation. The nitrogen species doubled the conductivity. On the one hand, nitrogen is an n-type dopant that modifies the electronic band structure of the carbon, thereby increasing the conductivity. On the other hand, during the synthesis the amount of resorcinol was kept constant, i.e., the additional melamine and formaldehyde increased the overall monomer concentration in the precursor solution. This resulted in more contact points between the microsphere units of the carbon aerogel, having also a positive effect on the electrical conductivity. Additionally, the 2D carbon layers increased the conductivity by a factor of 1.5 in both matrices.

3.2. Electrocatalytic performance

In order to reveal the potential of these carbon materials as electrodes in the ORR their electrochemical characteristics were investigated. The powdered electrode materials were tested in a three-electrode cell configuration. The corresponding cyclic voltammograms are presented in Fig 3. The experiments were recorded at 50 mV/s in Ar-bubbled 0.5 M H_2SO_4. All the curves have a slightly distorted rectangular shape indicating the contribution of the pseudo-faradic reactions of the corresponding O- and N groups [56]. In the case of the polymer derived aerogel samples the area of the voltammograms correlates well with S_{BET}, samples with higher surface area showing wider CV hysteresis (Table 4.). On the contrary, RGO exhibits outstandingly wide hysteresis despite its lower apparent surface area. The 30 min sonication applied during the ink preparation certainly resulted in further exfoliation of the few layer thick graphene units, increasing the actual surface area. Therefore the electrolyte has access to a higher surface than concluded from the nitrogen adsorption measurement with the BET model [57,58].

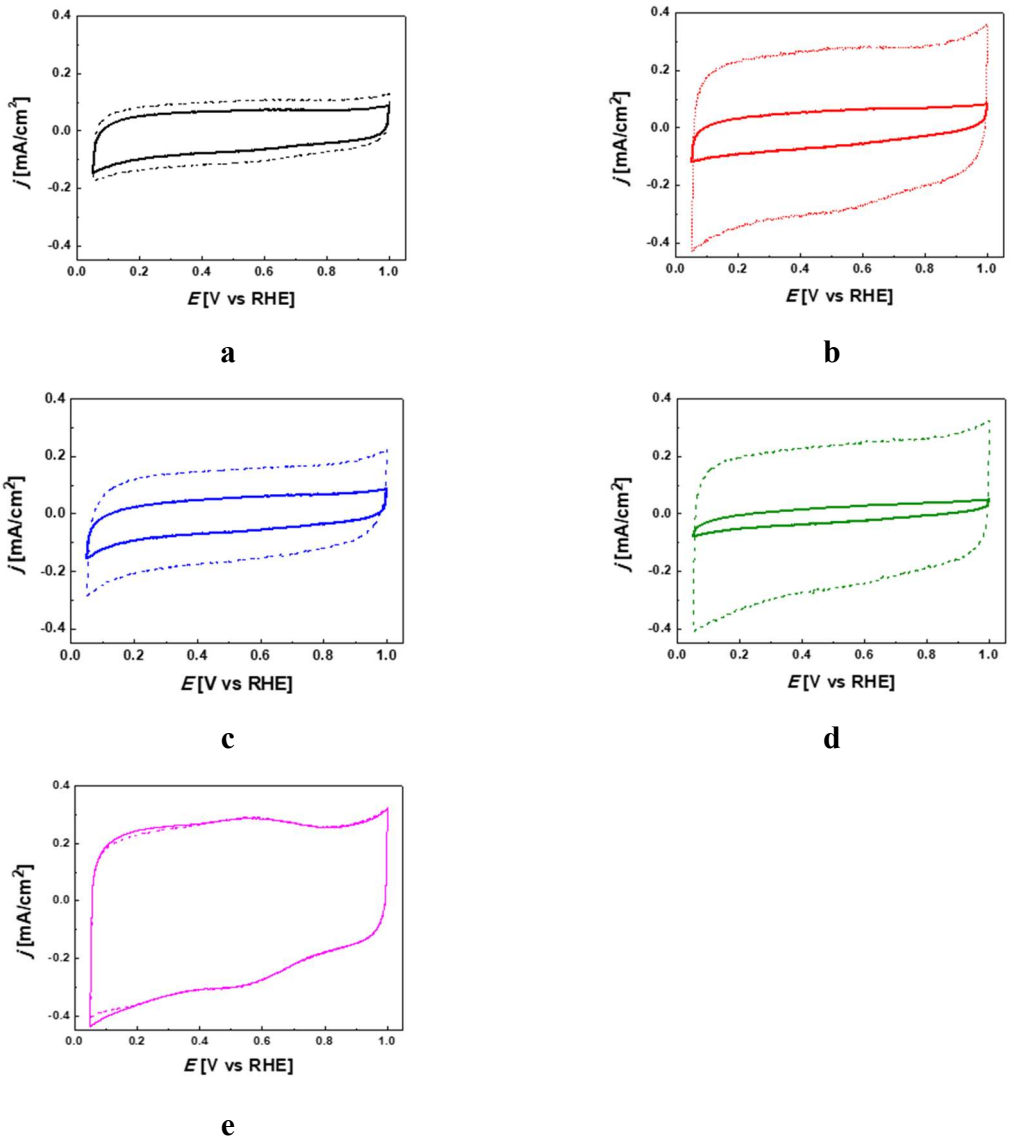

Fig. 3. Cyclic voltammograms of RFC (a), RFGC (b), RMFC (c), RMFGC (d) and RGO (e) measured in Ar-purged 0.5 M H_2SO_4 at scan rate 50 mV/s. Solid and dash lines were detected before and after the ORR tests, respectively.

The electrocatalytic properties were examined by a rotating disc electrode (RDE) in O_2-saturated 0.5 M H_2SO_4 electrolyte. As an illustration the polarization curves of RGO at different potentials and rotation rates (225-1225 rpm) are shown in Fig. 4. The LSV responses of the other samples are shown in Fig. S2 in the Supplement. At low potentials the current densities obviously depend on the rotating rates, indicating that the oxygen reduction is diffusion limited. The Koutecky-Levich (KL) equation was used to describe the correlation between the current densities and rotation rate

$$\frac{1}{j} = \frac{1}{j_k} + \frac{1}{j_{lim}} = \frac{1}{j_k} + \frac{1}{0.62nFCD^{\frac{2}{3}}\nu^{-\frac{1}{6}}\omega^{1/2}}, \qquad \text{(Eq. 1)}$$

where j is the current density, j_k is the kinetic current density, j_{lim} is the limiting diffusion current density, n is the number of electrons transferred in ORR per oxygen molecule, F is the Faraday constant (96486 C/mol), D is the diffusion coefficient of oxygen in electrolyte (1.4 10^{-5} cm^2/s), ν is the kinematic viscosity of the electrolyte ($1 \cdot 10^{-2}$ cm/s) and C is the concentration of oxygen in the electrolyte ($1.1 \cdot 10^{-6}$ mol/cm^3), the ω is the rotation rate in rad/s [59].

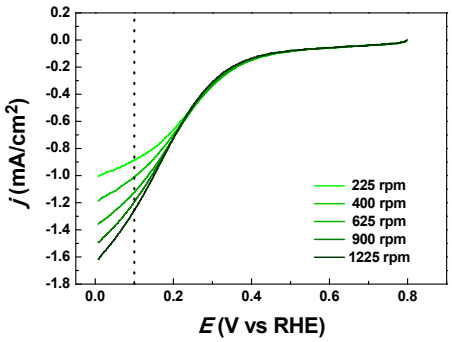

Fig. 4. Linear sweep voltammograms of RGO sample measured by rotating disk electrode (RDE). Measurements took place in O_2-saturated 0.5 M H_2SO_4 at scan rate 10 mV/s (b). Vertical line shows the j value for the KL plot. The LSV responses of the other samples are shown in Fig. S2 in the Supplement.

The KL plots are compared in Fig. 5a. All show a linear relationship between $1/j$ and $1/\omega^{1/2}$ at a potential of 0.1 V. The electron transfer number for the ORR can be estimated from the slope of this plot in spite of the complexity of the electrode processes [60]. The electrochemical reduction of O_2 is a multi-electron reaction that has two main possible pathways, as already pointed out in the Introduction section. For comparison, the theoretical KL plot of the two pathways is also plotted in Fig. 5. To obtain maximum energy capacity, it is highly desirable to reduce O_2 via the $4e^-$ pathway. According to the KL slopes in the case of samples RFC, RMFC and RFGC, mainly the slower, less efficient $2e^-$ route is taken. On the contrary the KL slopes corresponding to RMFGC and RGO electrode is close to the theoretical $4e^-$ route.

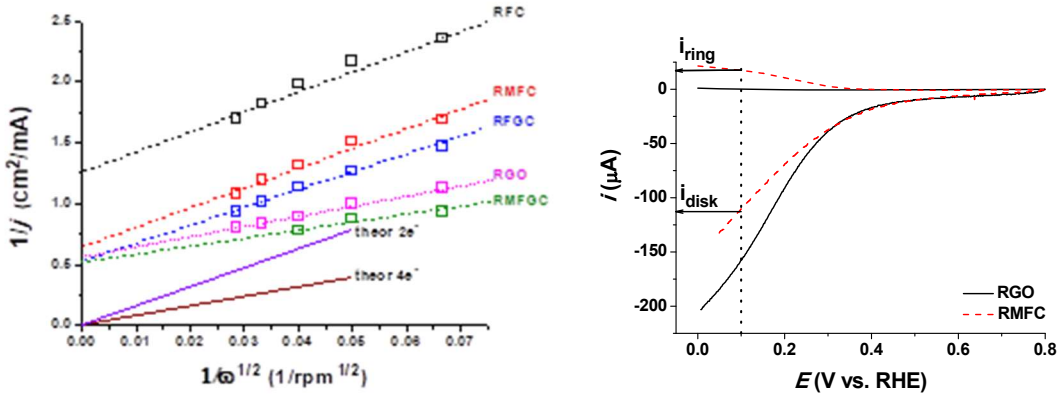

a b

Fig. 5. Koutecky-Levich plot of the carbon samples at 100 mV obtained from LSV measurements (a). Comparison of the current of the ring and disk measured by a rotating ring disk electrode (RRDE) (b). Vertical line shows the *j* value for the KL plot and *i* values for i_{ring}/i_{disk} comparison.

To verify these results the formation or the lack of H_2O_2 during the ORR process was monitored using rotating ring disk electrode as well. In Fig. 5b the simultaneously measured ring and disk currents are compared for the RMFC and RGO samples. While the ring current of RGO is negligible in the whole potential region measured, that of the RMFC sample is significant in the range where the ORR takes place. The i_{ring}/i_{disc} ratios read at 100 mV are tabulated in Table 4. The results are consistent with the data obtained from the slope of KL plots.

Table 4. Specific capacitance before and after ORR tests

Carbon sample	Estimated capacity*			Capacity change during ORR		$i_{ring}/i_{disk}\cdot 100$
	before ORR		after ORR			
	F/g	mF/m^{2*}	F/g	F/g	%	%
RFC	27	33	42	15	56	6
RFGC	25	31	106	81	324	7
RMFC	23	36	63	42	182	16
RMFGC	12	34	97	85	708	2
RGO	103	448	103	0	0	0

*capacity normalized to S_{BET}

Based on our results neither the presence of nitrogen nor the GO alone change the electrocatalytic behavior of the aerogel samples significantly. However, when both nitrogen and the remains of GO are present in the aerogel, the process becomes more efficient and the

dominant pathway changes from the $2e^-$ to the $4e^-$ route. Similar synergistic effect of nitrogen and another dopant, also in ORR process, has been recently reported [61].

Low temperature nitrogen adsorption measurements confirmed that the pore morphology was practically retained during H_2O_2 exposure. In order to follow the effect of the ORR on the electrode material the electrolyte was purged with Ar and CV was measured again after the ORR measurements (Fig 3, dashed lines). The electrochemical response of RGO did not change, but the CV of all the aerogel samples showed a significantly wider hysteresis, revealing increased capacities. The change is more expressed on the samples containing the graphene derivative. Both the shape of the voltammograms and the capacities become quite similar to those of the RGO. This phenomenon can be induced by two effects: i) the surface of the carbon gels is not stable and becomes activated with the H_2O_2 formed *in-situ*, ii) the *in-situ* formed H_2O_2 changes the surface chemistry and thus improves the wettability of the basically hydrophobic carbon surface. The latter may lead to the enhanced accessibility of the surface for the electrolyte, thereby expanding the electrochemically active surface. Our previous results showed that the peroxide treatment has no influence on the BET surface area. In order to confirm the modification of the surface chemistry powdered carbon samples were treated *ex situ* with 30 wt% H_2O_2 solution at ambient temperature. Two different approaches were applied. On the N and graphene free RFC samples the water vapour adsorption was measured before and after a 3 h treatment (Fig. S3). The increased slope of the initial section of the isotherm from 49 mg/g to 73 mg/g is a clear evidence of enhanced polarity and thus wettability [62]. The N and graphene doped RMFGC was artificially treated for 30 min. Carbon films were prepared from the aqueous suspensions of both the pristine and treated samples. Even the short reaction time was enough to modify the surface chemistry. The contact angle 139 ± 2 ° measured on the pristine RMFGC film decreased to 130 ± 3 ° after the H_2O_2 treatment (Fig. S4).

Conclusions

GO doped polymer aerogels without and with N content were synthesized and converted to carbon aerogels after their thermogravimetric analysis. The carbon aerogels were tested in oxygen reduction reaction (ORR). The influence of the evenly distributed GO on the polymer gel morphology is the most obvious in the micropore region. While addition of melamine to the precursor solution modifies the carbonization process, no influence of the added GO was observed. The N atoms from melamine are either converted to a C=N-C type chemical environment, or substitute a carbon atom in the graphene-like layer. Both N and the graphene not only enhance the electrical conductivity but all the samples are more active in ORR than

the RF itself. Nitrogen or the reduced GO alone do not change the mechanism of the electrocatalytic process. However, when both N and graphene are present in the matrix the dominant pathway changes from the slow $2e^-$ to the more efficient $4e^-$ route. The carbon aerogel samples are not stable during the ORR measurements but their capacities calculated from the cyclic voltammograms become much higher than before. The H_2O_2 formed *in-situ* improves the wettability of the basically hydrophobic carbon surface and fosters the accessibility of the surface for the electrolyte, thus increasing the electrochemically active surface.

Acknowledgement

The authors are grateful to E. Székely for her valuable contribution to supercritical drying and E. Albert for contact angle measurements. We thank Gy. Bosznai and G. Babos for their technical assistance. Financial support from the Hungarian Scientific Research Fund K109558 and VEKOP-2.3.2-16-2017-00013 is acknowledged. The VEKOP project is supported by the EU and by Hungary, co-financed by the European Regional Development Fund. The work is also part of the EU project NANOMED (H2020-MSCA-RISE-2016, #734641). The research reported in this paper was supported by the BME-Nanonotechnology FIKP grant of EMMI (BME FIKP-NAT).

References

[1] Andújar JM, Segura F. Fuel cells: History and updating. A walk along two centuries. Renew Sustain Energy Rev. 2009;13(9):2309–22.
[2] Wu H-W. A review of recent development: Transport and performance modeling of PEM fuel cells. Appl Energy. 2016;165:81–106.
[3] Shao Y, Sui J, Yin G, Gao Y. Nitrogen-doped carbon nanostructures and their composites as catalytic materials for proton exchange membrane fuel cell. Appl Catal B Environ. 2008;79(1):89–99.
[4] Yang Z, Nie H, Chen X, Chen X, Huang S. Recent progress in doped carbon nanomaterials as effective cathode catalysts for fuel cell oxygen reduction reaction. J Power Sources. 2013;236:238–49.
[5] Tardy GM, Lóránt B, Lóka M, Nagy B, László K. Enhancing substrate utilization and power production of a microbial fuel cell with nitrogen-doped carbon aerogel as cathode catalyst. Biotechnol Lett. 2017;39(7):993–9.
[6] Zhang L, Xia Z. Mechanisms of oxygen reduction reaction on nitrogen-doped graphene for fuel cells. J Phys Chem C. 2011;115(22):11170–6.
[7] Geng D, Chen Y, Chen Y, Li Y, Li R, Sun X, et al. High oxygen-reduction activity and durability of nitrogen-doped graphene. Energy Environ Sci. 2011;4:760–4.
[8] Wang X, Wang J, Wang D, Dou S, Ma Z, Wu J, et al. One-pot synthesis of nitrogen and sulfur co-doped graphene as efficient metal-free electrocatalysts for the oxygen reduction reaction. Chem Commun. 2014;50(37):4839–42.
[9] Stacy J, Regmi YN, Leonard B, Fan M. The recent progress and future of oxygen reduction reaction catalysis: A review. Renew Sustain Energy Rev. 2017;69:401–14.

[10] He Q, Cairns EJ. Recent progress in electrocatalysts for oxygen reduction suitable for alkaline anion exchange membrane fuel cells. J Electrochem Soc. 2015;162(14):1504–39.
[11] Dai L, Xue Y, Qu L, Choi H, Baek J. Metal-free catalysts for oxygen reduction reaction. Chem Rev. 2015;115(4823–4892).
[12] Voitko K V, Whitby RLD, Gun VM, Bakalinska OM, Kartel MT, Lászlo K, et al. Morphological and chemical features of nano and macroscale carbons affecting hydrogen peroxide decomposition in aqueous media. J Colloid Interface Sci. 2011;361(1):129–36.
[13] Voitko K, Tóth A, Demianenko E, Dobos G, Berke B, Bakalinska O. Catalytic performance of carbon nanotubes in H_2O_2 decomposition : Experimental and quantum chemical study. J Colloid Interface Sci. 2015;437:283–90.
[14] Guo D, Shibuya R, Akiba C, Saji S, Kondo T, Nakamura J. Active sites of nitrogen-doped carbon materials for oxygen reduction reaction clarified using model catalysts. Science (80-). 2016;351(6271):361–5.
[15] Zhu J, Xiao M, Song P, Fu J, Jin Z, Ma L, et al. Highly polarized carbon nano-architecture as robust metal-free catalyst for oxygen reduction in polymer electrolyte membrane fuel cells. Nano Energy. 2018;49:23–30.
[16] Borghei M, Lehtonen J, Liu L, Rojas OJ. Advanced Biomass-Derived Electrocatalysts for the Oxygen Reduction Reaction. Adv Mater. 2017;1703691:1–27.
[17] Sheng ZH, Shao L, Chen JJ, Bao WJ, Wang F Bin, Xia XH. Catalyst-free synthesis of nitrogen-doped graphene via thermal annealing graphite oxide with melamine and its excellent electrocatalysis. ACS Nano. 2011;5(6):4350–8.
[18] Liu G, Li X, Ganesan P, Popov BN. Studies of oxygen reduction reaction active sites and stability of nitrogen-modified carbon composite catalysts for PEM fuel cells. Electrochim Acta. 2010;55(8):2853–8.
[19] Liu H, Liu Y, Zhu D. Chemical doping of graphene. J Mater Chem. 2011;21(10):3335–45.
[20] Daems N, Sheng X, Vankelecom IFJ, Pescarmona PP. Metal-free doped carbon materials as electrocatalysts for the oxygen reduction reaction. J Mater Chem A. 2014;2(12):4085–110.
[21] Nagy B, Villar-Rodil S, Tascón JMD, Bakos I, László K. Nitrogen doped mesoporous carbon aerogels and implications for electrocatalytic oxygen reduction reactions. Microporous Mesoporous Mater. 2016;230:135–44.
[22] Baccile N, Laurent G, Coelho C, Babonneau F, Zhao L, Titirici M-M. Structural insights on nitrogen-containing hydrothermal carbon using solid-state magic angle spinning 13C and 15N nuclear magnetic resonance. J Phys Chem C. 2011;115:8976–8982.
[23] Yao L. Nitrogen-doped porous carbonderived from chitin with enhanced performances for oxygen reduction reaction and supercapacitor. Int J Electrochem Sci. 2018;13:5798–809.
[24] László K, Tombácz E, Kerepesi P. Surface chemistry of nanoporous carbon and the effect of pH on adsorption from aqueous phenol and. Colloids Surfaces A Physicochem Eng Asp. 2004;230:13–22.
[25] Lee KJ, Shiratori N, Lee HG, Miyawaki J, Mochida I, Yoon S, et al. Activated carbon nanofiber produced from electrospun polyacrylonitrile nanofiber as a highly efficient formaldehyde adsorbent. Carbon. 2010;48(15):4248–55.
[26] Zhao X, Ma X, Zheng P. The preparation of carboxylic-functional carbon-based nanofibers for the removal of cationic pollutants. Chemosphere. 2018;202:298–305.
[27] Liu G, Li X, Ganesan P, Popov BN. Environmental development of non-precious metal oxygen-reduction catalysts for PEM fuel cells based on N-doped ordered porous

carbon. Appl Catal B Environ. 2009;93:156–65.
[28] Nagaiah TC, Kundu S, Bron M, Muhler M, Schuhmann W. Nitrogen-doped carbon nanotubes as a cathode catalyst for the oxygen reduction reaction in alkaline medium. Electrochem commun. 2010;12(3):338–41.
[29] Grzyb B, Hildenbrand C, Berthon-Fabry S, Job N, Rigacci A, Achard P, et al. Functionalisation and chemical characterisation of cellulose-derived carbon aerogels. Carbon. 2010;48:2297–307.
[30] Seredych M, Hulicova-Jurcakova D, Qing G, Bandosz TJ. Surface functional groups of carbons and the effects of their chemical character , density and accessibility to ions on electrochemical performance. Carbon. 2008;46:1475–88.
[31] Lin YC, Lin CY, Chiu PW. Controllable graphene N-doping with ammonia plasma. Appl Phys Lett. 2010;96(13):133110–3.
[32] Bertóti I, Mohai M, László K. Surface modification of graphene and graphite by nitrogen plasma: Determination of chemical state alterations and assignments by quantitative X-ray photoelectron spectroscopy. Carbon. 2015;84(1):185–96.
[33] Pekala RW. Organic aerogels from the polycondensation of resorcinol with formaldehyde. J Mater Sci. 1989;24:3221–7.
[34] Pérez-Cadenas M, Moreno-Castilla C, Carrasco-Marín F, Pérez-Cadenas AF. Surface chemistry, porous texture, and morphology of N-doped carbon xerogels. Langmuir. 2009;25(1):466–70.
[35] Yang Y, Zhao B, Tang P, Cao Z, Huang M, Tan S. Flexible counter electrodes based on nitrogen-doped carbon aerogels with tunable pore structure for high-performance dye-sensitized solar cells. Carbon. 2014;77:113–21.
[36] Sousa JPS, Pereira MFR, Figueiredo JL. NO oxidation over nitrogen doped carbon xerogels. Appl Catal B Environ. 2012;125:398–408.
[37] Hao GP, Li WC, Qian D, Lu AH. Rapid synthesis of nitrogen-doped porous carbon monolith for CO2 capture. Adv Mater. 2010;22(7):853–7.
[38] Veselá P, Slovák V. Monitoring of N-doped organic xerogels pyrolysis by TG–MS. J Therm Anal Calorim. 2013;113(1):209–17.
[39] Frédéric Maillard, Pavel A. Simonov, Savinova. ER. Carbon materials as supports for fuel cells electrocatalysts in Carbon Materials for Catalysis. In: Serp P, José Luis Figueiredo, editors. Carbon materials for catalysis. John Wiley & Sons, Inc.; 2009. p. 429–81.
[40] Meng F., Zhang X., Xu B., Yue S., Guo H., Luo Y. Alkali-treated graphene oxide as a solid base catalyst: Synthesis and electrochemical capacitance of graphene/carbon composite aerogels. J Mater Chem. 2011;21(46):18537–9.
[41] Lee YJ, Park HW, Kim GP, Yi J, Song IK. Supercapacitive electrochemical performance of graphene-containing carbon aerogel prepared using polyethyleneimine-modified graphene oxide. Curr Appl Phys. 2013;13(5):945–9.
[42] Qian Y, Ismail IM, Stein A. Ultralight, high-surface-area, multifunctional graphene-based aerogels from self-assembly of graphene oxide and resol. Carbon. 2014;68:221–31.
[43] Zhang K, Ang T, Zhang L, Zhao S, Wu J. Pyrolyzed graphene oxide / resorcinol-formaldehyde resin composites as high-performance supercapacitor electrodes. Journal of Material Chemistry 2011;21:2163-2170.
[44] Ling Z, Wang G, Dong Q, Qian B, Zhang M, Li C, et al. An ionic liquid template approach to graphene–carbon xerogel composites for supercapacitors with enhanced performance. J Mater Chem A. 2014;2(35):14329.
[45] Zhang Y, Fan W, Huang Y, Zhang C, Liu T. Graphene/carbon aerogels derived from graphene crosslinked polyimide as electrode materials for supercapacitors. RSC Adv. 2015;5(2):1301–8.
[46] Sun Y, Li C, Shi G. Nanoporous nitrogen doped carbon modified graphene as

electrocatalyst for oxygen reduction reaction. J Mater Chem. 2012;22(25):12810–6.
[47] Marcano DC, Kosynkin D V, Berlin JM, Sinitskii A, Sun Z, Slesarev A, et al. Improved Synthesis of Graphene Oxide. ACS Nano. 2010;4(8):4806–14.
[48] Lin C, Ritter JA. Effect of synthesis pH on the structure of carbon xerogels. Carbon. 1997;35:1271–8.
[49] Czakkel O, Marthi K, Geissler E, László K. Influence of drying on the morphology of resorcinol–formaldehyde-based carbon gels. Microporous Mesoporous Mater. 2005;86(1–3):124–33.
[50] Zhang N, Qiu H, Si Y, Wang W, Gao J. Fabrication of highly porous biodegradable monoliths strengthened by graphene oxide and their adsorption of metal ions. Carbon. 2011;49(3):827–37.
[51] Devallencourt C, Saiter J, Fafet A, Ubrich E. Thermogravimetry/Fourier transform infrared coupling investigations to study the thermal stability of melamine formaldehyde resin. Thermochim Acta. 1995;259(1):143–51.
[52] Gonalves AG, Figueiredo JL, Órfão JJM, Pereira MFR. Influence of the surface chemistry of multi-walled carbon nanotubes on their activity as ozonation catalysts. Carbon. 2010;48(15):4369–81.
[53] Guo K, Song H, Chen X, Du X, Zhong L. Graphene oxide as an anti-shrinkage additive for resorcinol–formaldehyde composite aerogels. Phys Chem Chem Phys. 2014;16(23):11603–8.
[54] Ling Z, Wang G, Dong Q, Qian B, Zhang M, Li C, et al. An ionic liquid template approach to graphene–carbon xerogel composites for supercapacitors with enhanced performance. J Mater Chem A. 2014;2(35):14329.
[55] Thommes M, Kaneko K, Neimark A V., Olivier JP, Rodriguez-Reinoso F, Rouquerol J, et al. Physisorption of gases, with special reference to the evaluation of surface area and pore size distribution (IUPAC Technical Report). Pure Appl Chem. 2015;87(9–10):1051–69.
[56] Moreno-Castilla C, Dawidziuk MB, Carrasco-Marín F, Morallón E. Electrochemical performance of carbon gels with variable surface chemistry and physics. Carbon. 2012;50(9):3324–32.
[57] Hong An Wong C, Pumera M. Stripping voltammetry at chemically modified graphenes. RSC Adv. 2012;2(14):6068–72.
[58] Zhang W, He W, Jing X. Preparation of a stable graphene dispersion with high concentration by ultrasound. J Phys Chem B. 2010;114(32):10368–73.
[59] Chandran P, Ghosh A, Ramaprabhu S. High-performance Platinum-free oxygen reduction reaction and hydrogen oxidation reaction catalyst in polymer electrolyte membrane fuel cell. Sci Rep. 2018;8(1):1–11.
[60] Zhou R, Zheng Y, Jaroniec M, Qiao S-Z. Determination of the Electron Transfer Number for the Oxygen Reduction Reaction: From Theory to Experiment. ACS Catal. 2016;6(7):4720–8.
[61] Zhang J, Zhao Z, Xia Z, Dai L. A metal-free bifunctional electrocatalyst for oxygen reduction and oxygen evolution reactions. Nat Nanotechnol. 2015;10(5):444–52.
[62] László K, Czakkel O, Dobos G, Lodewyckx P, Rochas C, Geissler E. Water vapour adsorption in highly porous carbons as seen by small and wide angle X-ray scattering. Carbon. 2010;48(4):1038–48.